Deformation characteristics of tubular members with reference to impact loads from collision and dropped objects

By

*Tore H. Søreide , Jørgen Amdahl **
Division of Marine Structures
The Norwegian Institute of Technology, Trondheim
** On leave from Det norske Veritas*

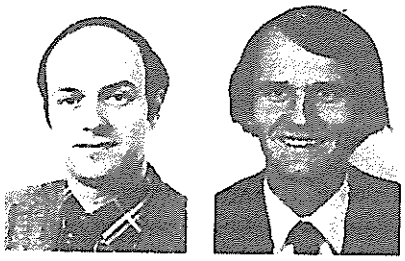

T. H. Søreide *Jørgen Amdahl*

Abstract

The paper deals with impact loads on tubular members. General impact mechanics for the case of ship/platform collision is presented together with analytical and numerical methods for estimating the energy absorption capability of bracing elements. Reductions in load carrying capacity of a simple tubular member due to ovalization and local crippling are discussed and incorporated in the numerical models.

A series of tests on tubular members is performed primarily to study two effects, namely the influence of membrane forces and dynamic loading. Both horizontally free and full axially restrained members are tested, and the increase in energy absorption due to membrane forces is demonstrated. The effect of membrane action on the type of collapse is also investigated.

Dynamic tests corresponding to a real velocity of 1.0—2.0 m per second are performed in order to study the influence of impact velocity on energy absorption capability.

Keywords: *Tubular members, impact, collision, dropped objects.*

1. INTRODUCTION

The implementation of accidental loads as a design limit state in offshore rules /1/ has strengthened the need for rational tools for such calculations. In connection with design and operation it is of interest to know the amount of damage to the structure as well as the residual strength in damaged condition.

Related to the prediction of damage due to impact loading, a new design philosophy is developed in the sense that structural capacity is given as energy absorbing capability ratner than as ultimate load. Design criteria are given as mass and impact velocity of a striking ship or the weight and drop height of objects. The aim of the calculation is first to predict the amount of damage to the structure and second to consider the structure in damaged condition exposed to environmental loads. The DnV rules for mobile offshore units /2/ specify 14 MJ (Mega Joule) as impact energy for sideway collision and 11 MJ for bow or stern collision, corresponding to a supply vessel of 5000 tonnes displacement with impact speed 2 m/sec. The weights of dropped objects are related to the operational hook loads in cranes. For special purpose structures the impact energy as given above may be modified and is subject to approval.

In order to get a representative model of a ship/platform collision deformation and energy absorbing characteristics of the two colliding bodies must be known. Pioneering work on the energy absorbing capability of ships has been carried out by Minorsky /3/ relating the amount of energy absorbed to the volume of damaged material. Most of the research on ships has been directed towards the protection of the reactor in nuclear powered ships /2/ and few attempts have been made to develop general analytical models for the deformation process.

The design of offshore platforms against collision is conservative in the sense that the striking ship is normally considered as undeformable so that the platform is designed to absorb all impact energy. For impact against a bracing element the deformation modes of the platform can conveniently be split into the following components:

a. Local deformation of tube wall at point of impact.
b. Beam deformation of bracing element.
c. Overall deformation of platform.

The first two modes involve considerable plastic energy absorption while the global response is mainly elastic, possibly with some dynamic effects involved. Normally the contribution to energy absorption from overall deformation can be neglected.

The transition between the different deformation modes is difficult to define. As a local dent is created in the tube wall the neutral axis changes, a phenomenon that is more associated with global beam deformation.

2. IMPACT MECHANICS

Consider the situation in Fig. 1 where collision between a supply vessel and a mobile semisubmersible platform is considered.

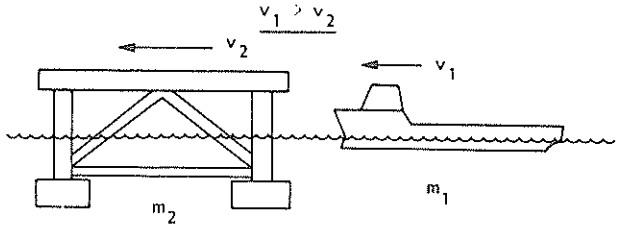

Fig. 1 Collision between supply vessel and semisubmersible platform.

The following notation is used in the subsequent derivations:

m_1 = mass of striking ship including added mass (40 percent of vessel displacement for sideway collision and 10 percent for bow or stern collision /2/).

m_2 = mass of semisubmersible platform including added mass

v_1 = velocity of striking ship immediately before collision

v_2 = velocity of semisubmersible platform immediately before collision

v_e = common velocity of ship and platform after impact

E_s = energy absorbed by ship

E_p = energy absorbed by platform

The derivation of a mathematical model of the ship/platform impact is based upon two criteria:
a. Conservation of momentum
b. Conservation of energy

The condition of momentum conservation is expressed by the following equation:

$$m_1 v_1 + m_2 v_2 = (m_1 + m_2) v_e \tag{1}$$

from which the common velocity after impact comes out as

$$v_e = \frac{m_1 v_1 + m_2 v_2}{m_1 + m_2} \tag{2}$$

The kinetic energy before impact to some extent dissipates through plastic deformation of ship and platform. The equation for energy conservation reads

$$\tfrac{1}{2} m_1 v_1^{\,2} + \tfrac{1}{2} m_2 v_2^{\,2} = \tfrac{1}{2}(m + m_2) v_e^{\,2} + E_s + E_p \tag{3}$$

Combining Eqs. (2, 3) the following expression for plastic energy dissipation emerges:

$$E_s + E_p = \tfrac{1}{2} m_1 v_1^{\,2} \cdot \frac{\left\{1 - \frac{v_2}{v_1}\right\}^2}{1 + \frac{m_1}{m_2}} \tag{4}$$

The above formula has been derived under the assumption that the effect of external forces from waves and mooring system can be neglected during impact.

It appears that if the two bodies have opposite directions of velocity prior to impact the amount of plastic energy to be absorbed may exceed the kinetic energy of the ship.

The corresponding expressions for collision against a fixed jacket type of structure are obtained by introducing $m_2 = \infty$, $v_2 = 0$ in Eq. (4):

$$E_s + E_p = \tfrac{1}{2} m_1 v_1^{\,2} \tag{5}$$

In the lack of reliable data for energy absorption in ships E_s is usually neglected, leading to a conservative design of platform structure.

The choice of design impact situations must be done under the consideration of probability of occurrence /5/. The size of design vessel is to be determined on the basis of the vessels intended to operate in the area such as service vessels, tankers for offshore loading and by-passing ships.

3. THEORETICAL MODELS FOR LOAD-DEFORMATION CHARACTERISTICS

3.1 LOCAL DEFORMATION OF TUBE WALL AT POINT OF IMPACT

The extent and form of local damage in the wall of a bracing element depends on the nature of impact. A head-on collision gives a more concentrated force than a sideway impact and results in a larger amount of local energy absorption of given mass and velocity of the vessel. Due to this complexity it is impossible to present one single analytical model for establishing local energy absorption. Several types of models have to be considered related to different collision situations.

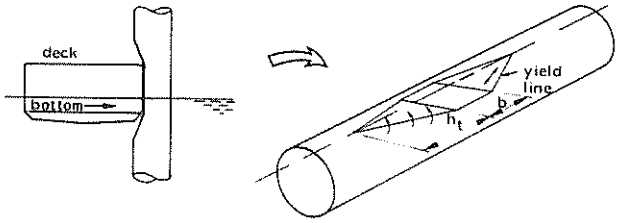

Fig. 2 Plastic mechanism for sideway impact by supply vessel.

For sideway impact a simple yield line model is presented by Furnes and Amdahl /5/, see also Fig. 2. The deformed surface is bounded by a series of yield lines and the following plastic effects are included:

a. Rotation of surface at yield lines
b. Flattening of surface between yield lines
c. Tension work due to elongation of generators

The theoretical model gives fairly good agreement with experimental results for small and medium identations. The model can form the basis for possible design curves when further verification against experiments has been performed.

3.2 ANALYTICAL TECHNIQUES FOR BEAM DEFORMATION

The rigid-plastic methods of analysis /6, 7, 8/ provide simple analytical results, often with acceptable accuracy and are appropriate for design situations. The simplest approach to the beam type of deformation is the three hinge mechanism, Fig. 3.

In the case of axially restrained ends the load carrying capacity of the beam increases considerably as the beam undergoes finite deflections due to the development of membrane tension forces. For a centrally loaded tubular beam the load-deflection relation is given by /9/

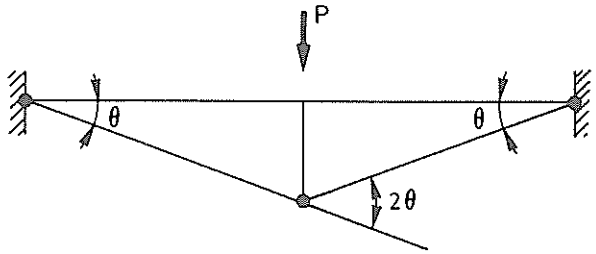

Fig. 3 Collapse mechanism for bracing element.

$$\frac{P}{P_0} = \sqrt{1 - \left(\frac{w}{D}\right)^2} + \frac{w}{D} \arcsin \frac{w}{D} \; ; \; \frac{w}{D} \leq 1 \tag{6}$$

$$\frac{P}{P_0} = \frac{\pi}{2} \frac{w}{D} \quad ; \; \frac{w}{D} > 1 \tag{7}$$

where w is the central deflection at the point of impact and D is the tube diameter. P_0 is the plastic collapse load of a circular tube in pure bending:

$$P_0 = \frac{8M_p}{\ell} = \frac{8\sigma_y D^2 t}{\ell} \tag{8}$$

The above expressions are based on the assumption that the ends have full axial restraint. In a real frame system like a jacket the bracing element sustains a certain degree of elastic support from the adjacent elements. Such elastic restrictions can be included by extending Hodge's method /6/ for the case of tubular members.

It is a major requirement for the validity of the present simple theory that no buckling of the tube wall takes place so that the full plastic capacity of the cross section is retained during deformation. Thus, restrictions must be set on maximum D/t-ratio for which the rigid-plastic theory can be used. Sherman /10, 11/ on the basis of tests on steel tubes in bending concluded that for members with D/t of 35 or less the full plastic moment is activated and sustained during deformation.

The API rules /12/ prescribe $D/t < 9000/\sigma_y$ (σ_y is yield stress in N/mm²) to maintain full capacity through plastic deformation. In the range $9000/\sigma_y < D/t < 15200/\sigma_y$ only a limited plastic rotation capacity can be presumed.

For the clamped ideally plastic element the absorbed plastic energy at any level of deflection w is found by integration of the load-displacement expressions in Eqs. (6, 7). The following energy expression emerges:

Geometric and material data for the models are given in Table 1. The range of variation is:

$$63 < D < 125 \text{ mm}$$
$$22 < D/t < 61$$
$$10 < L/D < 20$$
$$204 < \sigma_y < 328 \text{ N/mm}^2$$

where σ_y denotes yield stress according to uniaxial tensile tests.

SPECI-MEN	OUTER DIAMETER D mm	WALL THICKNESS t mm	D/t	LENGTH L mm	L/D	YIELD STRESS σ_y N/mm^2	STATIC OR DYNAMIC	HORIZ CONDIT
IAI	125	2.0	61	1244	10	264	Static	Free
IAII	125	2.0	61	1244	10	241	"	"
IAIII	125	2.0	61	1244	10	307	"	Fixed
IBI	125	2.5	50	1244	10	251	"	Free
IBII	125	2.5	50	1245	10	230	"	Fixed
IBIII	125	2.5	50	1245	10	268	"	Free
ICI	125	3.0	41	1245	10	268	"	"
ICII	125	3.1	40	1240	10	328	Dynamic	"
ICIII	125	3.1	41	1246	10	256	Static	Fixed
IDI	114	3.2	35	1240	11	318	"	"
IDII	114	3.2	35	1240	11	318	Dynamic	"
IEI	88	3.0	30	1240	14	294	Static	"
IEII	88	3.0	30	1240	14	294	Dynamic	"
IFI	63	2.9	22	1240	20	442	Static	"
IFII	63	2.9	22	1240	20	442	Dynamic	"

Table 1. Data for bracing models.

4.2 TEST RIG

The experimental set-up is shown in Fig. 9.

The hydraulic actuator is mounted on the upper transverse beam of the rig. The test specimen is fixed to each column in the way that a steel plate is welded to the ends of the tube and this plate is then bolted to a special arrangement which allows for various boundary conditions.

A better indication of the end conditions is given in Fig. 10. The rollers make it possible to simulate free horizontal movement as well as full membrane restraint. In both cases the tube end is rotationally clamped, which is assumed to be close to the real situation for a bracing element.

Displacement control of the hydraulic actuator is applied with a displacement rate of 0.15 mm per second for the static tests and 54 mm per second for dynamic testing which by scaling gives a real speed of 1.0—2.0 m per second. A rectangular indenter is used with a width (along bracing element) equal to 50 mm.

Strain gauges are placed close to the indenter where local deformation is expected and at the tube ends. Displacement transducers are mounted on each end to measure the horizontal movement and under the tube at the central section to register the vertical displacement of this point, which is to be compared with the movement of the top point given by the actuator.

4.3 STATIC TESTS

First, attention is given to the effect of membrane forces by considering the two specimens IAI and IAIII with equal geometric and material properties. Specimen IAI has horizontally free end conditions while IAIII is clamped against axial movement. Deformed configurations at different levels of loading are shown in Figs. 11 and 12 for IAI and IAIII, respectively. For specimen IAI it is seen that at maximum load carrying capacity the global deformation is small as compared with the local indentation (Fig. 11b). The effect of membrane forces is demonstrated by the difference in load carrying capacity. It is also seen that the stretching effect in specimen IAIII gives a much more overall ovalization of the tube than the very local cross-sectional deformation at point of impact for specimen IAI.

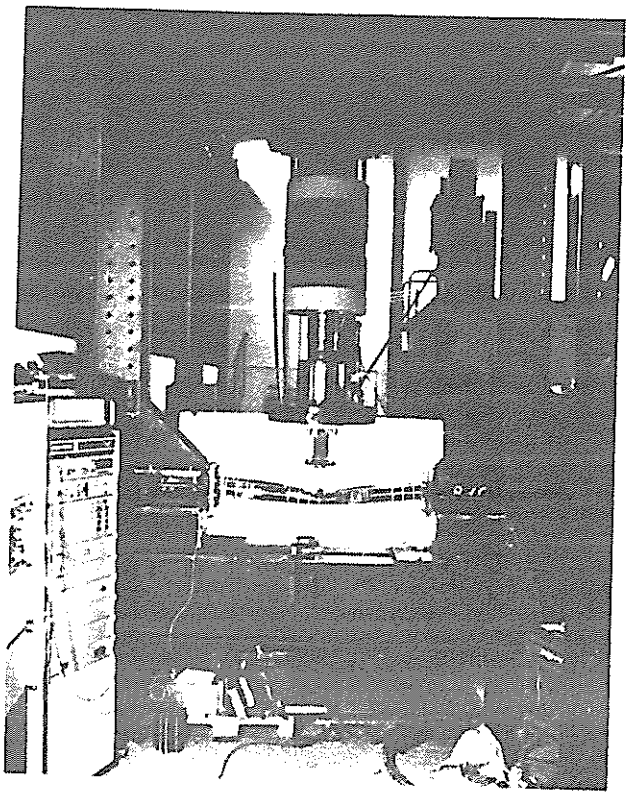

Fig. 9 Experimental set-up.

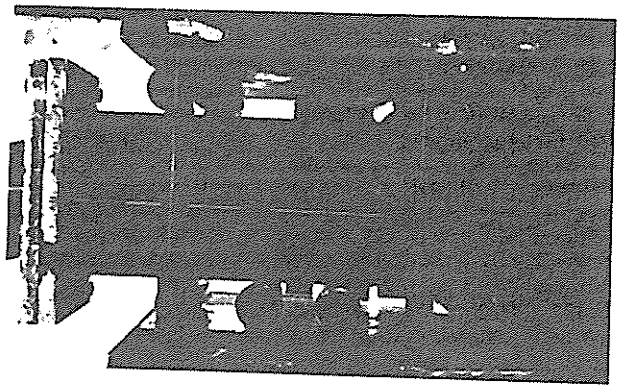

Fig. 10 End of test specimen.

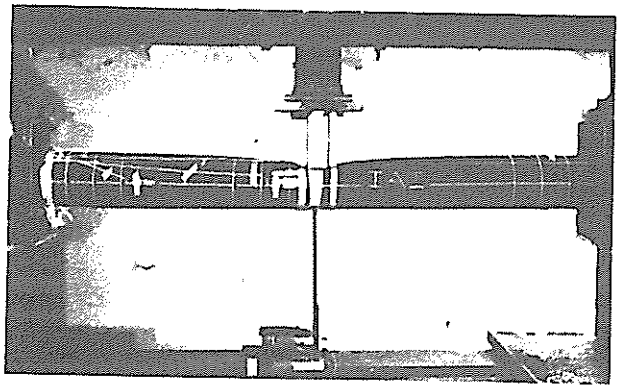

$P/P_0 = 0.50$

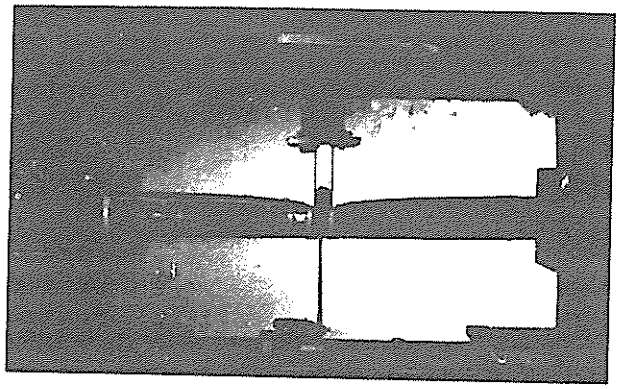

$P/P_0 = 0.64$

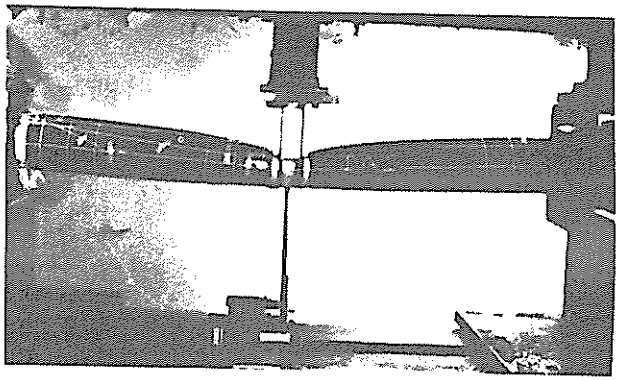

$P/P_0 = 0.69$

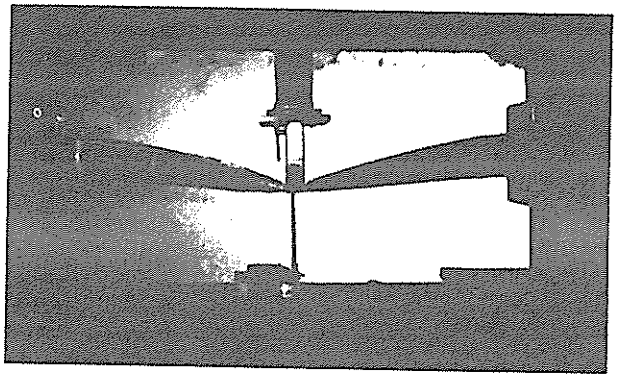

$P/P_0 = 1.44$

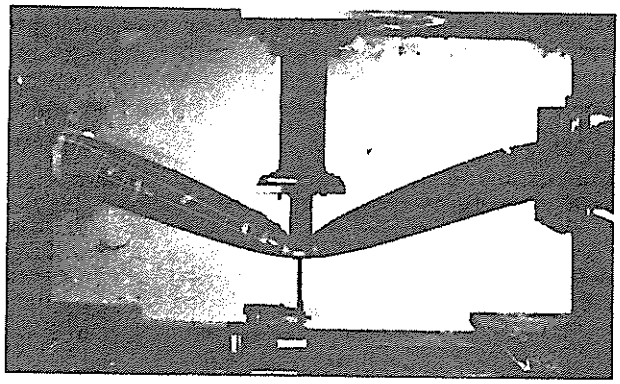

$P/P_0 = 0.46$

Fig. 11 Deformation of horizontally free specimen IAI.

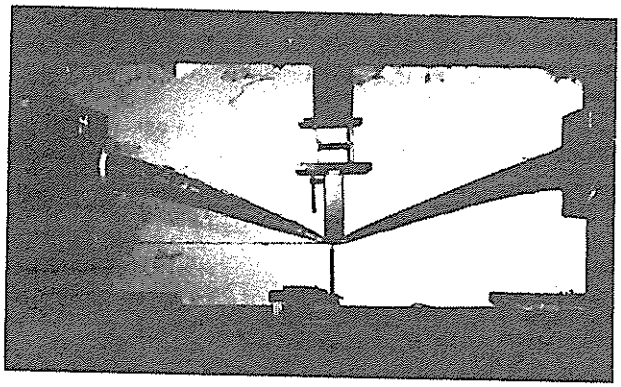

$P/P_0 = 3.50$

Fig. 12 Deformation of horizontally fixed specimen IAIII.

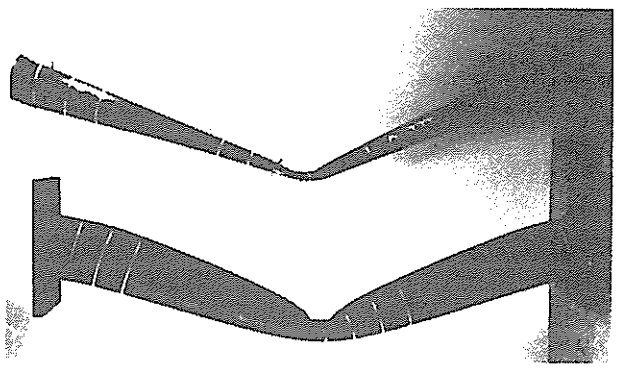

Fig. 13 shows the permanent deformation of IAI and IAIII after collapse. The axial elongation of specimen IAIII is clearly demonstrated by the difference in length between the two models.

The maximum indentation for the two specimens is close to 250 mm (2D).

The relationships between load and displacement

Fig. 13 Permanent deformation of specimens IAI and IAIII.

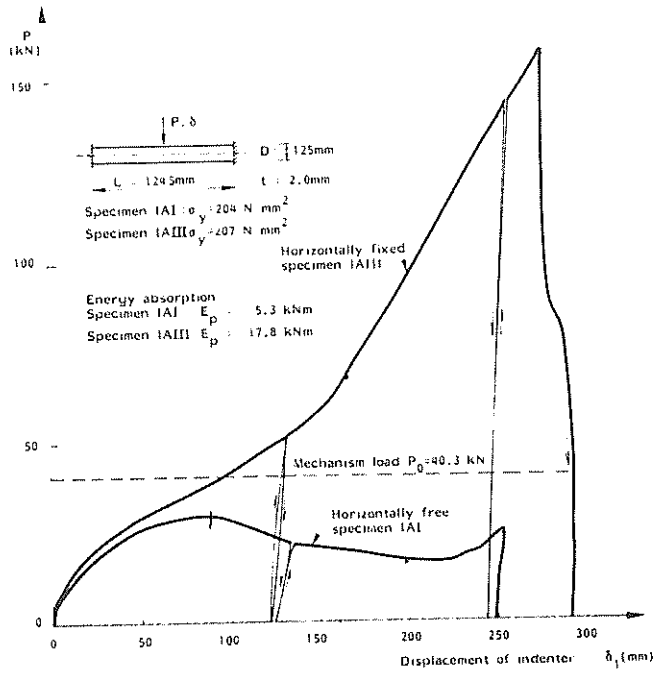

Fig. 14 Load-displacement curves for indenter. Specimens IAI and IAIII.

of indenter are given by the curves in Fig. 14. It is seen that the horizontally free specimen IAI reaches a a maximum load of 0.73 P_0 at an indentation of about 85 mm (δ/D = 0.68) where P_0 is the mechanism load as given by Eq. (8):

$$P_0 = \frac{8M_p}{L} = \frac{8D^2 t\sigma_y}{L} = 40 \text{ KN} \qquad (11)$$

t and L denote tube wall thickness and span, respectively. By further deformation of IAI the lateral load reduces to 0.40 P_0 (16 kN). The reason for this behaviour is twofold. First, due to the flattening of the central cross section the plastic section modulus is reduced. Second, local crippling of the tube wall is observed on the compression side of the ends (Fig. 15), an effect which also reduces the moment capacity.

In the final stage of deformation it is seen from Fig. 14 that the lateral load on specimen IAI rises as the first buckle at the ends closes and before the next buckle develops.

The load-displacement curve in Fig. 14 for specimen IAIII with membrane action is quite different. The load increases continuously and reaches an ultimate value of 4 P_0 (157 kN) before collapse. The energy absorbed is 17.8 kNm for IAIII versus 5.3 kNm for specimen IAI. The type of collapse of model IAIII is different from the horizontally free case.

Due to the membrane action the ends of specimen IAIII are in tension all over the cross section and no crippling occurs. Instead, the tube fails by fracture of the material close to the welds as shown in Fig. 16.

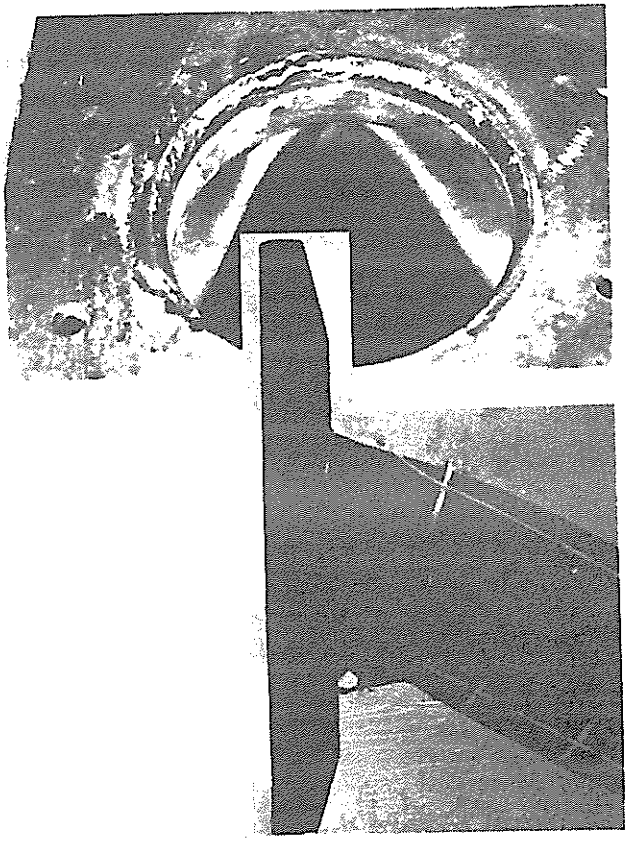

Fig. 15 Local crippling of tube wall at end of horizontally free specimen IAI.

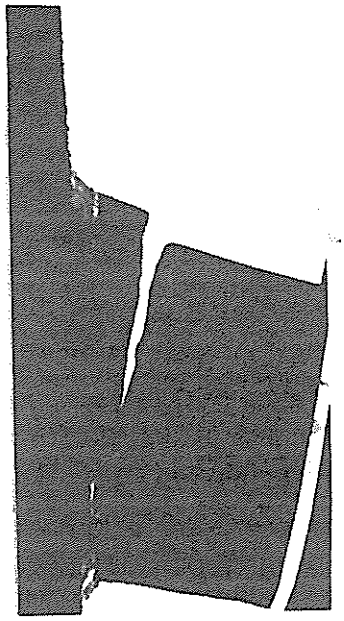

Fig. 16 Fracture at end of horizontally fixed specimen IAIII.

Although the present tests do not simulate the real behaviour of tubular joints some indications are obtained as far as type of collapse is concerned.

4.4 DYNAMIC TESTS

Consider the specimens IDI and IDII which are tested statically and dynamically, respectively with the deformation rates mentioned in Sect. 4.2. The load-displacement curves are shown in Fig. 17 where series 1 of curves is given for the indentation on the upper side of the specimens and the series 2 is related to the displacement transducer on the opposite side of the central cross section.

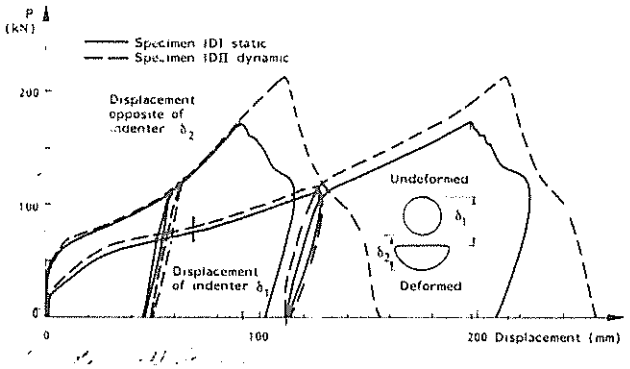

Fig. 17 Static and dynamic load-displacement curves.

Fig. 17 shows that the load-indentation curve (series 1) is raised by about 10 percent due to the dynamic loading, while very little influence is obtained on the opposite side of the cross section (series 2). This phenomenon indicates that the dynamic loading primarily affects the local deformation at point of impact with its high concentration of yield hinges, and that the increase in load carrying capacity is caused by a rise in the material stress-strain curve. However, it should be emphasized that this conclusion is representative only for the present range of impact velocity. Inertia forces may change the dynamic influence for higher velocities.

5. COMPARISON BETWEEN TEST RESULTS AND THEORY

One special problem arises when relating the test results to theoretical load-displacement curves, namely the choice of reference displacement. The analytical rigid-plastic technique of Sect. 3.2 and the modified elasto-plastic computer program of Sect. 3.3 both refer to lateral deflection w as the centre line displacement while mid-section deflection is measured on top and bottom of the tube.

In order to make test results and theoretical solutions compatible the measured top and bottom

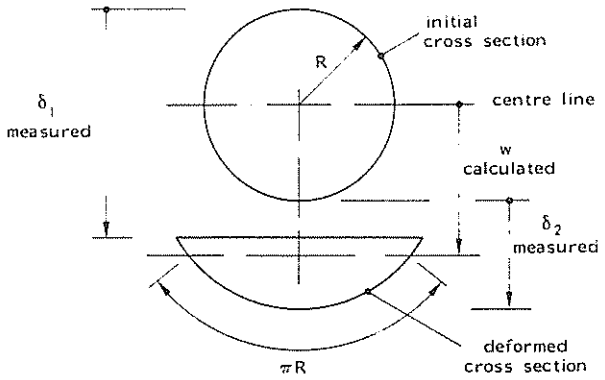

Fig. 18 Calculation of centre line deflection.

displacements δ_1 and δ_2 are transformed into centre deflection w via the model in Fig. 18. The deformed cross section at point of impact is approximated by a horizontal part and a circular part with increased radius of curvature, similar to the model used in Fig. 4 for calculating reduced section modulus. Incorporating the requirement of constant circumference during deformation of the cross section w can be calculated and now denotes physically the displacement of points on centre line.

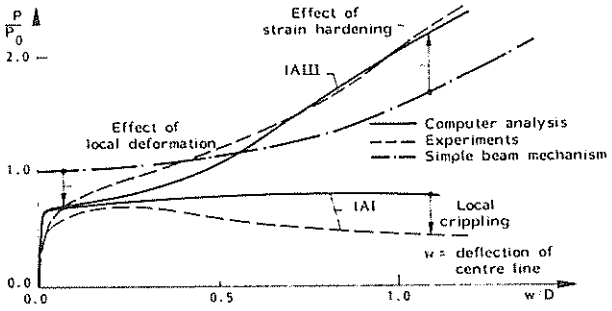

Fig. 19 Load-deflections characteristics for specimens IAI and IAIII.

Fig. 19 shows the transformed test results and the theoretical load-deflection curves. It is seen that the modified beam computer program IMPACT with strain hardening included fairly well follows the experimental deflection for the horizontally fixed specimen IAIII. Some discrepancy arises through the development of local dent in the first phase of deformation. Also for the horizontally free specimen IAI the maximum load is well predicted by the program. However, since full rotational rigidity is assumed at the tube ends, the unloading due to local crippling does not come out of the numerical analysis. For specimen IAI it is also clear that the simple mechanism model neglecting local deformation of cross section gives too high load carrying capacity.

The part of energy absorption due to global beam

deformation is found as the area under the load-deflection curves in Fig. 19. Further, the energy absorbed by local dent plastification must be calculated separately and added to the global contribution to obtain the total energy absorption capability as given by Fig. 14. In the computer program IMPACT the calculation of local energy absorption is carried out by the local indentation program part b of Sect. 3.3.

6. CONCLUSIONS

Theoretical methods to calculate the energy absorption capability of tubular steel members have been assessed by comparison with experiments. It is clear that the weakening effect of local indentation on the global strength must be taken into consideration.

The test included horizontally free members as well as elements with full axial restraint. The membrane forces clearly affected the deformation characteristics and type of collapse. In the cases with free horizontal movement the elements failed by local crippling of the tube wall on the compression side of the ends. For the axially restrained members total collapse was caused by fracture close to the welds. Special studies on tubular joints have to be performed in order to obtain more information about their capacity under various types of loading.

Dynamic tests with a velocity corresponding to 1.0-2.0 m per second in full scale indicated an increase in load carrying capacity of about 10 percent as compared with static tests. Most of this reserve was due to change in material properties in the region of local indentation.

REFERENCES

/ 1/ Det norske Veritas: Rules for the Design, Construction and Inspection of Offshore Structures, 1977.

/ 2/ Det norske Veritas: Rules for Classification of Mobile Offshore Units, 1981.

/ 3/ Minorsky, V. V.: «An Analysis of Ship Collisions with Reference to Nuclear Power Plants», J Journ. of S hip Research, Vol. 3, 1959, pp. 1—4.

/ 4/ Woisin, C.: «Die Kollisionsversuche der GKSS», Jahrbuch der Schiffbautechnischen Gesellshaft, 70.8, Hamburg 1976.

/ 5/ Furnes, O. and Amdahl, J.: «Ship Collisions with Offshore Platforms», Intermaritec, Hamburg, 1980.

/ 6/ Hodge, Ph.G.: «Post-Yield Behaviour of a Beam with Partial End Fixity», International Journal of Mechanical Sciences, Vol. 16, 1974, pp. 385—388.

/ 7/ Jones, N.: «Plastic Behaviour of Ship Structures», Transactions Society of Naval Architects and Marine Engineers, Vol. 84, 1976, pp. 115—145.

/ 8/ Guedes Soares, C. and Søreide, T. H.: «Large Plastic Deformation of Laterally Loaded Circular Tubes», Division of Marine Structures, The Norwegian Institute of Technology, Trondheim, Norway, 1982.

/ 9/ Søreide, T. H.: «Ultimate Load Ananlysis of Marine Structures», Tapir Publishing Company, Trondheim, Norway, 1981.

/10/ Sherman, D. R. and Glass, A. M.: «Ultimate Bending Capacity of Circular Tubes», OTC 2119, pp. 901—910.

/11/ Sherman, D. R.: «Tests of Circular Steel Tubes in Bending», ASCE J. Struct. Div., Vol. 102, No. ST11, 1976, pp. 2181—2195.

/12/ American Petroleum Institute: Recommended Practice for Planning, Designing and Constructing Fixed Offshore Platforms, API RP 2A, 1979.

/13/ Søreide, T. H.: «IMPACT — A Computer Program for Non-linear Geometric and Material Analysis of Beams and Columns», Division of Marine Structures, The Norwegian Institute of Technology, Trondheim, Norway 1981.

/14/ Remseth, S. N., Holthe, K., Bergan, P. G. and Holand, I.: «Tube Buckling Analysis by the Finite Element Method», Finite Elements in Nonlinear Mechanics, Tapir Publishing Company, Trondheim, Norway 1977.

/15/ Søreide, T. H.: «Collapse Behaviour of Stiffened Plates using Alternative Finite Element Formulations, Dr. ing. Thesis, Division of Structural Mechanics, The Norwegian Institute of Technology, Trondheim, Norway, 1977.

/16/ Yura, J. A., Zettlemoyer, N. and Edwards, I. F.: «Ultimate Capacity Equations for Tubular Joints», OTC 3690, 1980.